Cell Tissue Res (2013) 352:707–725
DOI 10.1007/s00441-013-1615-9

REGULAR ARTICLE

Role of the subcommissural organ in the pathogenesis of congenital hydrocephalus in the HTx rat

Alexander R. Ortloff · Karin Vío · Montserrat Guerra · Katherine Jaramillo · Thilo Kaehne · Hazel Jones · James P. McAllister II · Esteban Rodríguez

Received: 12 November 2012 / Accepted: 8 March 2013 / Published online: 4 May 2013

Abstract The present investigation was designed to clarify the role of the subcommissural organ (SCO) in the pathogenesis of hydrocephalus occurring in the HTx rat. The brains of non-affected and hydrocephalic HTx rats from embryonic day 15 (E15) to postnatal day 10 (PN10) were processed for electron microscopy, lectin binding and immunocytochemistry by using a series of antibodies. Cerebrospinal fluid (CSF) samples of non-affected and hydrocephalic HTx rats were collected at PN1, PN7 and PN30 and analysed by one- and two-dimensional electrophoresis, immunoblotting and nanoLC-ESI-MS/MS. A distinct malformation of the SCO is present as early as E15. Since stenosis of the Sylvius aqueduct (SA) occurs at E18 and dilation of the lateral ventricles starts at E19, the malformation of the SCO clearly precedes the onset of hydrocephalus. In the affected rats, the cephalic and caudal thirds of the SCO showed high secretory activity with all methods used, whereas the middle third showed no signs of secretion. At E18, the middle non-secretory third of the SCO progressively fused with the ventral wall of SA, resulting in marked aqueduct stenosis and severe hydrocephalus. The abnormal development of the SCO resulted in the permanent absence of Reissner's fibre (RF) and led to changes in the protein composition of the CSF. Since the SCO is the source of a large mass of sialilated glycoproteins that form the RF and of those that remain CSF-soluble, we hypothesize that the absence of this large mass of negatively charged molecules from the SA domain results in SA stenosis and impairs the bulk flow of CSF through the aqueduct.

Keywords Hydrocephalus · Subcommissural organ · Reissner's fibre · Cerebrospinal fluid · HTx rat

A.R. Ortloff and K. Vío should be considered as first authors.

This work was supported by grants from Fondecyt (Chile) to E. Rodríguez (nos. 1070241 and 1111018), a Hydrocephalus Association Established Investigator Award to E. Rodríguez and J.P. McAllister (no. 51002705), a grant from Universidad Austral de Chile/DID S-2006-72 to K. Vío and a Conicyt PhD Fellowship to A.R. Ortloff.

A. R. Ortloff · K. Vío · M. Guerra · K. Jaramillo · E. Rodríguez (✉)
Instituto de Anatomía, Histología y Patología, Facultad de Medicina, Universidad Austral de Chile, Valdivia, Chile
e-mail: erodrigu@uach.cl

A. R. Ortloff
Escuela de Medicina Veterinaria, Universidad Católica de Temuco, Temuco, Chile

T. Kaehne
Institute of Experimental Internal Medicine, Otto-von-Guericke University Magdeburg, Leipziger Strasse 44-0, 39120 Magdeburg, Germany

H. Jones
Gagle Brook House, Chesterton, Bicester OX 1UF, UK

J. P. McAllister II
Division of Pediatric Neurosurgery, Department of Neurosurgery, Medical School, University of Utah, Salt Lake City UT 84132, USA

Introduction

The subcommissural organ (SCO) is an ependymal gland located at the roof of the third ventricle, at the entrance to the mesencephalic aqueduct. Ependymal SCO cells continuously secrete high molecular mass glycoproteins into the cerebrospinal fluid (CSF) in which the bulk of them condense to form a filamentous structure, named Reissner's fibre (RF; Rodríguez et al. 1992, 1998). The RF is a dynamic structure that continuously grows caudally by the addition of newly released molecules to its cephalic end. SCO-spondin has been identified as the main glycoprotein of RF (Gobron et al. 2000; Meiniel 2001). The RF extends through the aqueduct of

Sylvius (SA), the fourth ventricle and the central canal of the spinal cord to reach the ampulla caudalis or fifth ventricle located at the end of the central canal. Here, the RF disassembles at a constant rate (Rodríguez et al. 1992, 1998) and RF-glycoproteins reach local blood vessels (Peruzzo et al. 1987). RF has the capacity to bind and transport compounds such as monoamines and contributes to the clearance of these compounds from the CSF (Rodríguez et al. 1999; Rodríguez and Caprile 2001; Caprile et al. 2003).

The SCO differentiates at an early stage of ontogenetic development in all vertebrates and, with the exception of anthropoids and bats, it remains fully active throughout life (Rodríguez et al. 1998, 2001). Ontogenetic studies have revealed signs of secretory activity in SCO cells much earlier than the appearance of the first RF (Schoebitz et al. 1986, 1993; Rodríguez et al. 1998). In the rat, the SCO is well developed and is immunoreactive with anti-RF antibodies at embryonic day 14 (E14). However, aggregated secretory material and a RF proper first appear during the first postnatal week (Schoebitz et al. 1993). These findings indicate that the embryonic SCO secretes compounds that remain soluble in the CSF (Hoyo-Becerra et al. 2006; Vío et al. 2008). Evidence exists that SCO secretes transthyretin (TTR), a protein involved in the transport of thyroid hormones in the CSF (Montecinos et al. 2005).

Several mutant rodent models developing congenital hydrocephalus have revealed the role of the neuroepithelium/ependymal cells and those of the SCO in the onset of fetal hydrocephalus (Wagner et al. 2003; Chae et al. 2004; Huh et al. 2009). Transcription factors, such as the regulatory factor X (Rfx) family, Msx1 and Pax 6, have been identified as key factors involved in dorsal neural patterning (Estivill-Torrus et al. 2001; Fernández-Llebrez et al. 2004; Baas et al. 2006; Zhang et al. 2007). Abnormalities in these developmental factors impair SCO formation and function and trigger fetal-onset hydrocephalus. Increasing evidence also implicates signal transduction mechanisms in the processes regulating SCO secretion as a cause of hydrocephalus (Lang et al. 2006; Picketts 2006). Further, a single injection of antibodies against RF-glycoproteins disrupts RF formation in the adult rat (Rodríguez et al. 1990) and immunological blockage of the SCO-RF complex by maternal transfer of anti-RF antibodies triggers SA stenosis and hydrocephalus (Vío et al. 2000).

The HTx rat is a genetic model of fetal-onset hydrocephalus with a complex mode of inheritance (Jones et al. 2004) and with confounding epigenetic influences (Jones et al. 2002). In the HTx rat, stenosis of the SA and dilation of the lateral ventricles start to occur around E18 (Jones and Bucknall 1988); this is preceded by reduced glycoprotein immunoreactivity in the SCO at E16 (Somera and Jones 2004). The mechanism and sequence of neuropathological events leading to SA obliteration are not known. The present investigation has been designed to investigate the SCO-RF complex of non-affected (nHTx) and hydrocephalic (hyHTx) littermates, with the aim of (1) analysing the SCO-RF complex at various developmental periods, (2) investigating the proteins secreted by the SCO into the CSF and (3) gaining evidence of the role of SCO-RF complex in SA obliteration and pathogenesis of hydrocephalus. The evidence obtained indicates that, in the hyHTx rat, the abnormal development and dysfunction of the SCO precedes the development of hydrocephalus.

Materials and methods

Animals

Rats of the HTx strain were obtained from the laboratory of Dr. Hazel Jones (University of Florida) in 2002 and were bred into a colony in the animal house of the Instituto de Anatomía, Histología y Patología, Universidad Austral de Chile, Valdivia, Chile. The rats were fed *ad libitum* with rodent food and maintained under a constant 12-h light/12-h dark photoperiod and room temperature of 25°C. The colony was maintained by brother-sister mating of non-affected non-hydrocephalic rats. To obtain embryos and fetuses at various developmental stages, brother-sister pairs of non-hydrocephalic HTx rats were caged together for mating. Every morning vaginal smears were performed in order to find spermatozoids in the vaginal tract to determine the exact day of copulation. A sequential morphological analysis of the brain of embryos from E15 to E21 was performed (see below). The day of birth was considered to be postnatal day 1 (PN1). The hydrocephalic phenotype was identified from an overtly domed head and by trans-illumination of the head. The definitive diagnosis was made by microscopic analysis. Handling, care and processing of animals were carried out according to regulations approved by the National Research Council of Chile (Conicyt), the council of the American Physiological Society and the Institutional Animal Care and Use Committee of the University of Utah.

Animals for light microscopical analysis

Embryos (n=120; at E15, E16, E17, E18, E19, E20, and E21) were collected and processed. Because the hydrocephalic phenotype could not be recognized before E18, the brains of all embryos from E15 to E17 (before SA stenosis) were serially sectioned and analysed microscopically. The abnormal phenotype of the SCO was found to be expressed as early as E15. This landmark was used to characterize an embryo as having the hydrocephalic phenotype. Seventy-nine embryos were classified as nHTx and 41 were classified as hyHTx. Twenty-five neonatal rats (at PN1, PN3, PN5, PN7 and PN10) were classified as hyHTx and 36 rats were classified as nHTx. All rats belonging to the same litter were processed

simultaneously, allowing a comparative analysis of nHTx and hyHTx littermates of the same age. Pregnant and newborn rats were weighed and anaesthetized with an intraperitoneal injection of ketamine (40 mg/kg) and acepromazine (100 mg/kg). The head was cut off and a sagittal cut through the lateral region of the skull was performed to expose the brain tissue. Fixative was injected into a lateral ventricle. The head was then immersed in Bouin's fixative for 20 min. The brain was dissected, immersed in fresh fixative for 2 days and embedded in paraffin. Serial sagittal or transverse sections (5 μm thick) of the central nervous system were obtained. The brains of 40 hyHTx and 40 nHTx rats were cut serially. Each series contained about 300 sections; every tenth section of the series was mounted on separate and successive slides, thus giving ten semi-series of sections that were used for immunocytochemistry. In the remaining 75 nHTx and 16 hyHTx rats, adjacent serial sections through the SCO-aqueduct region were mounted separately and used for immunocytochemistry and lectin binding.

Immunocytochemistry

The peroxidase-antiperoxidase (PAP) method of Sternberger et al. (1970) was applied. The following primary antibodies were used. (1) The AFRU (A = antibody, FR = Reissner's fibre, U = urea; Instituto de Anatomía, Histología y Patología, Universidad Austral de Chile) antibody was raised in rabbits against the constitutive glycoproteins of the bovine RF and specifically reacts with the high-molecular-weight glycoproteins secreted by the SCO into the CSF. AFRU was used at a dilution of 1:1000. (2) Anti-nestin is a monoclonal antibody raised in mouse (Rat-401, Hybridoma bank of Iowa University) and was used at a dilution of 1:50. Incubation in the primary antibody was for 18 h. Sections to be immunoreacted with anti-nestin were incubated in 0.02 M citrate buffer, pH 6.0, followed by microwave irradiation for three sessions of 4 min each. Anti-rabbit IgG raised in goats (Instituto de Anatomía, Histología y Patología, Universidad Austral de Chile) and anti-mouse IgG (Sigma, Madrid, Spain) were used at a dilution 1:50 for 1 h. PAP complexes obtained by using anti-peroxidase developed in rabbits (Instituto de Anatomía, Histología y Patología, Universidad Austral de Chile) or mouse (DAKO, Barcelona, Spain) were used at a dilution of 1:50 and 1:100, respectively, for 30 min. DAB (3,3′-diaminobenzidine tetrahydrochloride; Sigma, St. Louis, Mo., USA) was used as an electron donor. Incubations were performed at 20°C. All antibodies were diluted in 0.1 M TRIS buffer, pH 7.8, containing 0.7% non-gelling seaweed gelatine lambda carrageenan and 0.5% Triton X-100 (both from Sigma). Omission of the incubation in the primary antibody was used as a control for the immunoreaction.

Double-immunofluorescence and confocal microscopy

For double-immunofluorescence, sections were incubated overnight at room temperature with primary antibodies (raised in rats or rabbits) for 18 h. The following pairs of antibodies were used: RAFRU (rat AFRU, dilution 1:500)/anti-caveolin 1 (rabbit polyclonal antibody, dilution 1:50; Santa Cruz) and AFRU (dilution 1:1000)/anti-β-tubulin IV (monoclonal antibody, dilution 1:50; Abcam, UK). After being washed in TRIS buffer, pH 7.8, sections were incubated with Alexa-488-labeled anti-rabbit IgG and Alexa-594-labeled anti-mouse IgG antibodies (Invitrogen, Carlsbad, Calif., USA) diluted 1:500 for 2 h. All antisera were diluted in TRIS buffer, pH 7.8, containing 0.7% nongelling seaweed carrageenan (Sigma) and 0.5% Triton X-100 (Sigma). Slides were coverslipped by using Vectashield mounting medium (Dako, Barcelona, Spain) and inspected under an epifluorescence microscope to study colocalization by using the multidimensional acquisition software AxioVision Rel version 4.6 (Zeiss, Aalen, Germany). Confocal microscopy was performed on some sections used for immunofluorescence by using a Fluoview 1000 (Miami, Fla., USA) laser-scanning microscope.

Lectin binding

Three lectins were used: (1) wheat germ agglutinin (WGA; affinity: internal residues of glucosamine and sialic acid residues); unlabelled WGA (Sigma) dissolved in 0.1 M TRIS Ca Mg buffer, pH 7.6, was used at a concentration of 7 μg/ml; (2) Concanavalin A (ConA; affinity: internal residues of mannose and glucose); unlabelled ConA (Sigma) dissolved in TRIS Ca Mg buffer, pH 7.6, was used at a concentration of 7 μg/ml; (3) *Limax flavus* agglutinin (LFA; affinity: exclusively for sialic acid); unlabelled LFA (Calbiochem, San Diego, Calif., USA) dissolved in 0.1 M TRIS Ca Mg buffer, pH 7.6, was used at a concentration of 7 μg/ml. Incubation in lectins was for 1 h at 22°C. Lectin binding was followed by incubation with the corresponding antibody, namely, anti-WGA (Sigma), anti-ConA (Sigma) or anti-LFA (Instituto de Anatomía, Histología y Patología, Universidad Austral de Chile) used at a dilution of 1:1000. The PAP method was applied and DAB (Sigma) was used as an electron donor.

Double-labelling with antibodies and lectins

For double-labelling, sections were incubated overnight at room temperature with an antibody raised in rats against RF-glycoproteins labelled by RAFRU, at a 1:500 dilution. After being washed in TRIS buffer, pH 7.8, sections were incubated with Alexa-488-labeled anti-rat IgG antibodies (Invitrogen) diluted 1:500 for 2 h. Following further washes

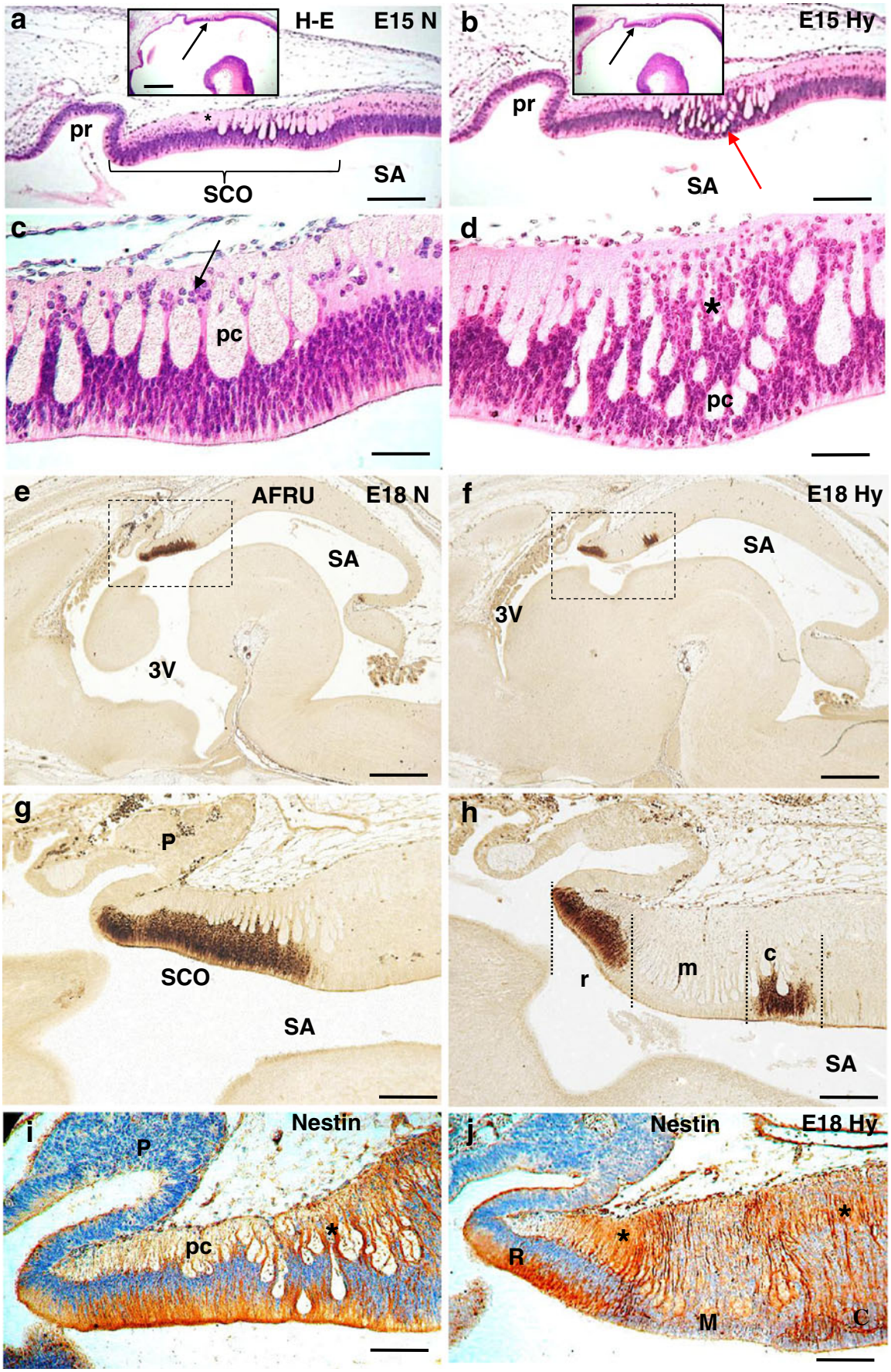
a
H-E
E15 N
pr
*
SCO
SA
b
E15 Hy
pr
SA
c
pc
d
*
pc
e
AFRU
E18 N
SA
3V
f
E18 Hy
SA
3V
g
P
SCO
SA
h
r
m
c
SA
i
Nestin
P
pc
*
j
Nestin
E18 Hy
*
*
R
M
C

◀ **Fig. 1** Subcommissural organ (*SCO*) of non-affected and hydrocephalic HTx rats. The hydrocephalic HTx rat displays abnormalities before the onset of hydrocephalus. **a**, **c** Midsagittal section through the pretectum and Sylvian aqueduct (*SA*) of a non-affected embryo (*N*) at embryonic day 15 (*E15*). Staining with haematoxylin and eosin (*H-E*). The SCO and the pineal primordium (*pr*) is morphologically differentiated (*pc* posterior commissure cells). The ependymal cells of the SCO project basal processes that end on the external limiting membrane of the brain and are associated with small clusters of cells of unknown nature (**c**, *arrow*). *Inset* in **a** Low-power view of telencephalon showing the SCO (*arrow*). **b**, **d** Midsagittal section through the pretectum and SA of an abnormal embryo (*Hy*) at E15. Staining with H-E. In the middle third of the rostro-caudal axis, the ependymal cells of the SCO are much smaller compared with those of the rostral and caudal thirds (**b**, **d**, *red arrow*). In the middle third, the bundles of commissural axons are smaller and more numerous and are located closer to the ependymal layer (compare **a**, **c** with **b**, **d**). Clustered cells of an unknown nature are associated with the commissural axons (compare **c**, *arrow* and **d**, *asterisk*). *Inset* in **b** Low-power view of telencephalon showing the SCO (*arrow*). **e**–**h** Midsagittal sections of SCO of nHTx (**e**, **g**) and hyHTx rats at E18 (**f**, **h**), immunostained with AFRU (A = antibody, FR = Reissner's fibre, U = urea). The SCO of nHTx rats is well developed, strongly immunoreactive and producing secretions (**e**, **g**), whereas the abnormality of the SCO of hyHTx rats (**f**, **h**) becomes evident (*3V* Third ventricle, *P* pineal gland, *r* rostral, *m* middle, *c* caudal). **i**, **j** Midsagittal sections of SCO of normal E18 rat (**i**) and abnormal E18 HTx rat (**j**) immunostained with anti-nestin. The basal processes of the ependymal cells of the SCO are strongly immunostained in the nHTx rat (**i**, *asterisk*). In the hyHTx rat, only the basal processes of the rostral and caudal third of the SCO are immunostained (**j**, *asterisks*; *R* rostral, *M* middle,). *Bars* 125 μm (**a**, **b**), 450 μm (*insets*), 50 μm (**c**, **d**), 480 μm (**e**, **f**), 125 μm (**g**, **h**), 100 μm (**i**, **j**)

with TRIS buffer, pH 7.8, sections were incubated with unlabelled LFA (7 μg/ml; Calbiochem) dissolved in 0.1 M TRIS Ca Mg buffer, pH 7.6, for 1 h at 22°C. Lectin binding was revealed by sequential incubation of sections with anti-LFA at a dilution of 1:1000, for 18 h and Alexa-594-labeled anti-rabbit IgG antibodies (Invitrogen) diluted 1:500, for 2 h. After washes in TRIS buffer, pH 7.8, slides were coverslipped by using Vectashield mounting medium (Dako) and inspected under an epifluorescence microscope to study colocalization by using the multidimensional acquisition software AxioVision Rel version 4.6 (Zeiss).

Transmission electron microscopy

Once the light microscopy analysis and the characterization of the embryos with an abnormal phenotype were completed, the SCO and SA of four nHTx and four hyHTx rats (at E18 and PN1) were processed for transmission electron microscopy. Brain tissue from pregnant and newborn rats was prepared as for light microscopy (see above), except that a triple aldehyde fixative mixture containing 4% paraformaldehyde, 2% glutaraldehyde, 2% acrolein in 0.2 M phosphate buffer, pH 7.4, was used. A sagittal cut through the lateral region of the skull was performed to expose the brain tissue. Fixative was gently subperfused into the exposed brain cavities by using a microliter syringe. The head was immersed in the same fixative for 20 min and the brain was dissected out and immersed again in the fixative for 2 h. Blocks of tissue containing the SCO and rostral third of the SA were obtained and fixed in 1% OsO_4 in 0.1 M phosphate buffer, pH 7.4, for 2 h at 4°C. They were subsequently embedded in Epon. Sections were contrasted with lead citrate and uranyl acetate and analysed under a Hitachi H-700 electron microscope.

CSF collection

Non-affected and hydrocephalic HTx rats at PN1 (nHTx n=60; hyHTx n=30), PN7 (nHTx n=50; hyHTx n=30) and PN30 (nHTx n=60; hyHTx n=20) were used for CSF collection. Pups at PN1 and PN7 were anaesthetized with ketamine (40 mg/kg) and acepromazine (100 mg/kg), the head was flexed and a 27-gauge needle was inserted into the cisterna magna (non-affected and hydrocephalic pups; CM-CSF) and lateral ventricles (hydrocephalic pups; LV-CSF). In PN30 rats, CM-CSF was collected from non-affected and hydrocephalic rats and LV-CSF was collected from hydrocephalic animals according to Rodríguez et al. (1999). CSF samples containing blood were discarded. About 25–50 μl CSF were obtained from each pup and up to 100 μl from each PN30 rat. CSF samples were collected into Eppendorf tubes and centrifuged twice to remove cells or cell debris. Average protein concentrations of PN1, PN7 and PN30 CSF samples were 1.8, 1.0 and 0.8 μg/μl, respectively. Samples were stored at −70°C until analysis.

One-dimensional electrophoresis and immunoblotting

Sodium dodecyl sulfate polyacrylamide gel electrophoresis (SDS-PAGE) was performed according to the Laemmli method. Briefly, 15 μl undiluted/non-concentrated CSF samples from PN1, PN7 and PN30 rats were subjected to SDS-PAGE by using a 5%–15% polyacrylamide linear gradient. Proteins were transferred to nitrocellulose membranes (Towbin et al. 1979). To block non-specific binding, blots were saturated with 5% non-fat milk in 0.1 M phosphate-buffered saline containing 0.15 mM NaCl and 0.1% Tween-20 (Sigma, Madrid, Spain), for 90 min. AFRU (1:5000 dilution) and anti-TTR (1:3000 dilution, Sigma) were used as primary antibodies. Anti-rabbit IgG conjugated to horseradish peroxidase (Pierce, Rockford, Ill., USA) was used at a 1:25,000 dilution, for 1.5 h. Incubations were carried out at room temperature in the dark. Immunoreactive polypeptides were detected by using an enhanced chemiluminescence (ECL) system (Super Signal;

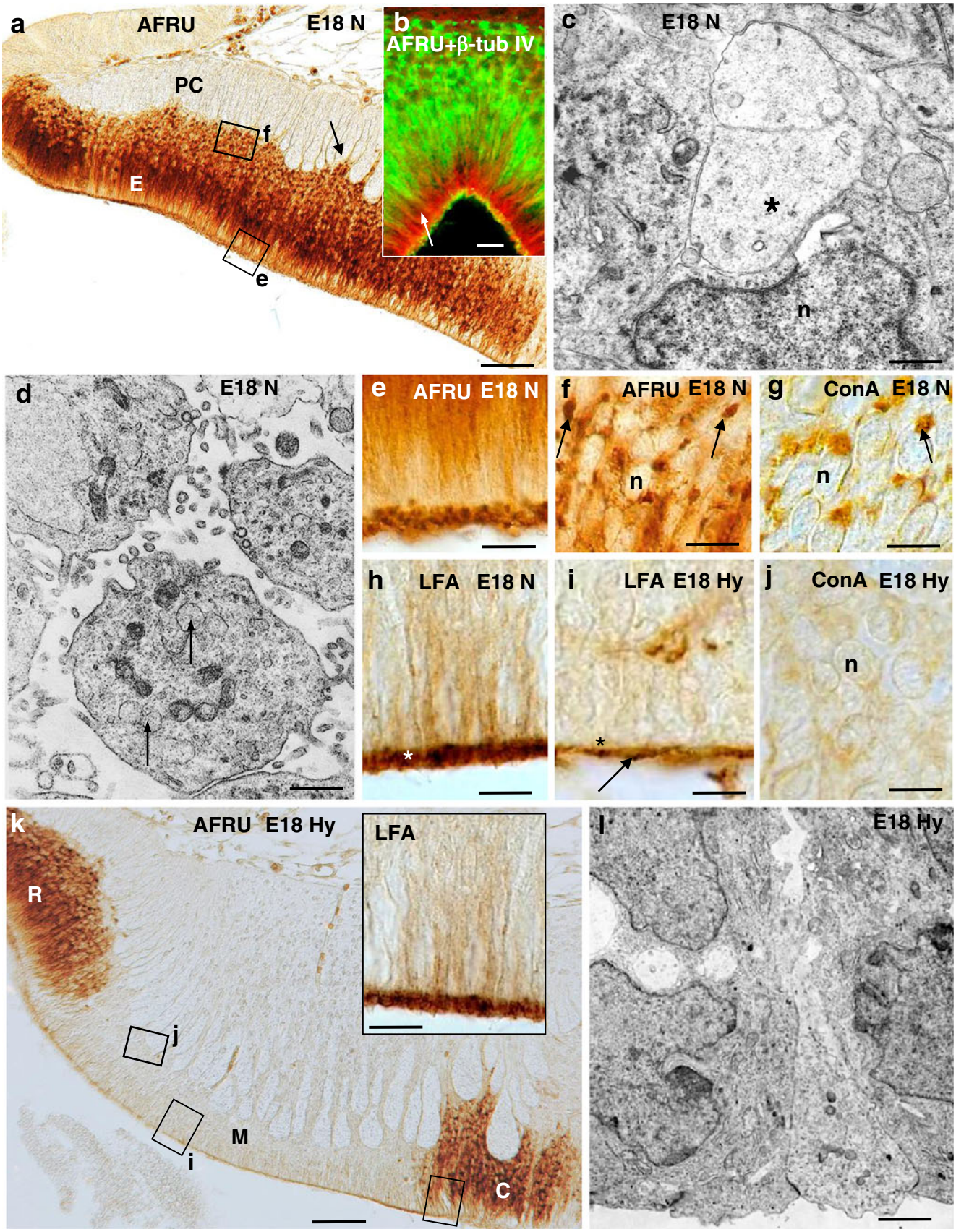
a
AFRU
E18 N
PC
E
f
e
b
AFRU+β-tub IV
c
E18 N
n
d
E18 N
e
AFRU E18 N
f
AFRU E18 N
n
g
ConA E18 N
n
h
LFA E18 N
i
LFA E18 Hy
j
ConA E18 Hy
n
k
AFRU E18 Hy
R
LFA
j
M
i
C
l
E18 Hy

◀ **Fig. 2** SCO of the non-affected HTx rat is fully differentiated at E18. **a** All secretory ependymocytes (*E*) of the SCO of a non-affected embryo are strongly immunoreactive with AFRU (*PC* posterior commissure). The basal processes of these cells contain AFRU+ material (*arrow*). **b** Double-immunolabelling with AFRU (*green*) and anti-βIV-tubulin (*red*) shows the subapical zone (*arrow*) devoid of secretion and containing microtubules (*red*). **c** Ultrastructure of the subnuclear zone containing large rough endoplasmic reticulum (RER) cisternae (*asterisk*); *n* cell nucleus. **d** Ultrastructure of the apical cell poles containing secretory granules (*arrows*). **e** Details of the *boxed area* in **a**. Subapical and apical zones of the SCO cells are immunostained with AFRU. Granules stored in the apical cell pole are AFRU+. **f** Details of the *boxed area* in **a**. **f**, **g** The subnuclear region of SCO cells display AFRU+ (**f**, *arrows*) and ConA+ (**g**, *arrow*) structures most likely corresponding to dilated RER cisternae (*n* cell nucleus). **h** Subapical and apical zones of the SCO cells. Granules stored in the apical cell pole are LFA+ (*white asterisk*). **i** Detail of *boxed area* in **k**. Subapical and apical zones of the SCO cells. LFA+ granules are missing (*black asterisk*). A thin LFA+ glycocalyx is seen (*arrow*). **j** Detail of *boxed area* in **k**. LFA+ RER cisternae are absent. **k** Rostral (*R*) and caudal (*C*) thirds are formed by secretory ependymocytes similar to those of non-affected E18 embryos with regard to AFRU immunoreactivity and LFA binding. The middle third (*M*) is formed by ependymal cells that are shorter, lack basal long processes and do not react with AFRU. *Inset* Area similar to that showed in *rectangle i* processed for LFA binding. **l** Under the electron microscope, these cells do not display signs of secretory activity. Secretory granules are absent. *Bars* 50 μm (**a**), 15 μm (**b**), 1.5 μm(**c**), 2 μm(**d**), 10 μm(**e**, **h**, **i**), 14 μm (**f**), 10 μm (**g**), 10 μm (**j**), 50 μm (**k**), 10 μm (*inset*), 4 μm (**l**)

Pierce) as instructed by the manufacturer. Molecular weight standards in the range of 10–250 kDa were used (Bio-Rad, Hercules, Calif., USA). Control blots were processed as above without the primary antibody. Immunoblots were digitized (n=4 for each condition analysed) and densitograms were obtained by using UN-SCAN-IT software (Silk Scientific, Orem, Utah, USA). Statistical analyses were performed by using Prism software (GraphPad Software, San Diego, Calif., USA) with 1-way analysis of variance (ANOVA) and Tukey's test.

Two-dimensional electrophoresis and immunoblotting

Isoelectric focusing (IEF) was carried out with a PROTEAN IEF Cell electrophoresis system (Bio-Rad). CSF samples from PN1, PN7 and PN30 rats were used for analytical runs. Briefly, 50 μg protein, contained in 50 μl CSF, was mixed with a rehydration solution containing 8 M urea, 2% CHAPS, 0.5% carrier ampholytes (Bio Lyte 3-10 buffer; Bio-Rad), 18 mM dithiothreitol (DTT) and a trace of bromophenol blue, in a total volume of 300 μl and applied to immobilizing pH gradient gels (ReadyStrip IPG Strips; 7 cm, 3-10 NL, Bio-Rad). After passive rehydration for 14 h at 20°C, IEF was performed as follows: linear 500 V for 30 min, rapid 1000 V for 1 h. For two-dimensional (2D) gel electrophoresis, focused strip gels were reduced by equilibrating for 30 min in equilibration buffer containing 64.8 mM DTT and then alkylated by equilibrating for 30 min in 135 mM iodoacetamide. SDS-PAGE was performed according to the Laemmli method until the bromophenol blue dye front reached the bottom of the gel. After SDS-PAGE, gels were silver-stained (Shevchenko et al. 1996) or transferred to nitrocellulose membranes for immunoblotting as previously described. Silver-stain spots were digitized (n=37 for each condition analysed) and densitograms were obtained by using UN-SCAN-IT software (Silk Scientific). Since the density of the group of spots labelled as "spot 35" was consistently similar in CSF samples from non-affected and hydrocephalic animals (see below), this density was regarded as 100% to evaluate the increase or decrease in the density of other spots that showed variability. Statistical analyses were performed by using Prism software (GraphPad Software) with 1-way ANOVA and Tukey's test.

In-gel digestion and nanoLC-ESI-MS/MS analyses

In-gel digestion Spots from 2D gels stained with silver nitrate were excised and digested in-gel in an adapted manner according to Shevchenko et al. (1996).

Mass spectrometric analysis Dried samples were dissolved in 10 μl 2% acetonitrile (ACN)/0.1% trifluoroacetic acid (TFA) and applied to an Ultimate 3000 Nano-HPLC (Dionex, Germany). Each sample was first trapped on a 1-mm PepMap-trapping column (Dionex, Germany) for 10 min at 30 μl/min 2% ACN/0.1% TFA and subsequently subjected to a 75-μm ID, 5 cm PepMap C18-column (Dionex, Germany). Peptide separation was performed by an ACN-gradient at 300 nl/min under the following conditions: 0–40 min: 2%–50% ACN, 0.1% formic acid; 40–50 min: 50%–90% ACN, 0.1% formic acid; 50–55 min: 90% ACN, 0.1% formic acid; 55–70 min: 2% ACN, 0.1% formic acid. The separation column outlet was online-coupled to a nano-spray interface (Bruker, Germany) of an Esquire HCT ETDII-Iontrap mass spectrometer (Bruker, Germany). Mass spectra were acquired in positive mass spectrometric (MS)-mode, tuned for tryptic peptides. MS/MS-precursor selection was performed in an optimized automatic regime, with preference for double- and triple-charged ions. Every selected precursor was fragmented by collision-induced dissociation (CID) and electron transfer dissociation (ETD). MS/MS spectra were processed by the Data Analysis and BioTools software from Bruker, Germany. Combined CID/ETD-derived fragment lists were analysed by the MASCOT algorithm on the swissprot-database.

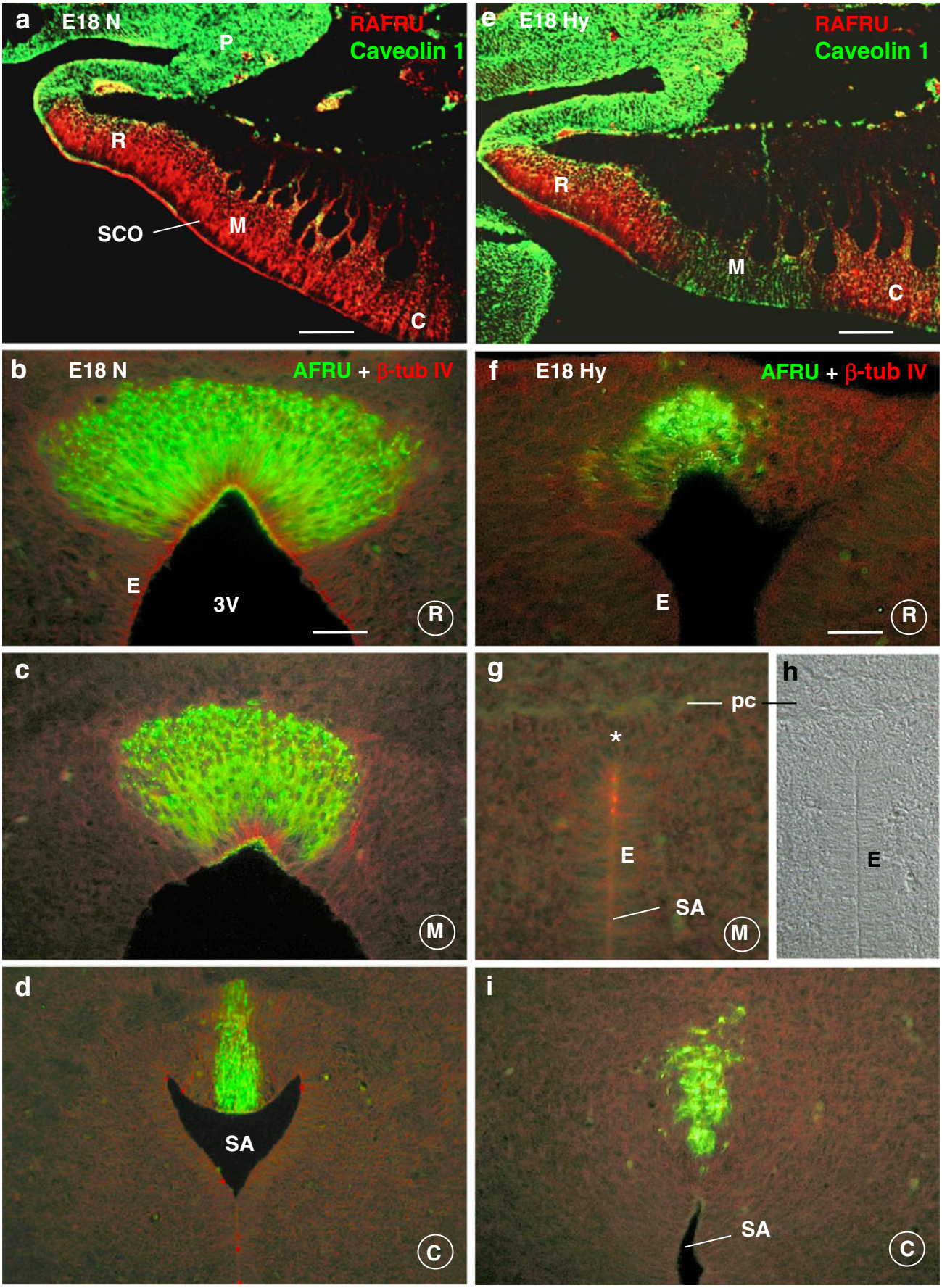
a
E18 N
RAFRU
Caveolin 1
P
R
SCO
M
C
e
E18 Hy
RAFRU
Caveolin 1
R
M
C
b
E18 N
AFRU + β-tub IV
E
3V
R
f
E18 Hy
AFRU + β-tub IV
E
R
c
M
g
pc
*
E
SA
M
h
E
d
SA
C
i
SA
C

◀ **Fig. 3** SCO of hydrocephalic HTx rat displays distinct abnormalities at E18, before onset of hydrocephalus. The three regions of the SCO of a non-affected (*N*) and an hydrocephalic HTx rat (*Hy*) are shown in sagittal and frontal sections (*pc* posterior commissure, *E* ciliated ependymal cells). Double-immunolabeling with rat AFRU (RAFRU; *red*) and anti-caveolin 1 (*green* in **a**, **e**) or with AFRU (*green*) and anti-β-tubulin IV (*red* in **b**, **c**, **d**, **f**, **g**, **i**). In the nHTx rat, secretory ependymocytes of the rostral (*R*), middle (*M*) and caudal (*C*) regions of the SCO are strongly reactive with AFRU and anti-caveolin 1 (**a**). In the hydrocephalic HTx rat, SCO ependymocytes of the middle region react with anti-caveolin 1 but not with AFRU (**e**). **b–d** Frontal sections through the three regions shown in **a**, revealing the secretory ependymocytes in the three regions. **f–i** Frontal sections through the three regions shown in **e**. SCO-ependymocytes of the rostral (**f**) and caudal (**i**) regions strongly react with AFRU. AFRU+ cells are absent in the middle region (**g**, *asterisk*). **h** Section through the middle region of the SCO visualized with Nomarski optics showing the absence of SCO cells and marked stenosis of the Sylvian aqueduct (*SA*). *Bars* 80 μm (**a**, **e**), 40 μm (**b**, **c**, **d**, **f**, **g**, **i**)

Results

SCO-RF complex of non-affected and hydrocephalic HTx fetuses before onset of hydrocephalus at E18

Non-affected HTx fetuses Staining with haematoxylin-eosin and immunostaining with AFRU of the semi-series of sections through the brain of nHTx HTx fetuses killed before onset of hydrocephalus revealed that the pretectum was morphologically differentiated at E15 (Fig. 1a). Large bundles of axons forming the posterior commissure and crossing the midline had been formed by this time (Fig. 1c). At E15, the SCO first displayed immunoreactivity with AFRU, an antibody specific for the glycoproteins secreted by SCO cells. By E17 and E18, the SCO of the nHTx fetuses was strongly reactive with AFRU (Fig. 1e, g). Ependymocytes of the SCO displayed the well-known zonation of the cytoplasm (Fig. 2a). The subnuclear zone displayed large cisternae of rough endoplasmic reticulum (RER; Fig. 2c) reacting with AFRU and binding the lectin ConA (Fig. 2f, g). The supranuclear zone of ependymocytes contained the Golgi apparatus, numerous cisternae of RER and immature AFRU-positive (AFRU+), ConA+ secretory granules (Fig. 2a, b). The subapical zone of SCO ependymocytes contained a few secretory granules and microtubules that were strongly reactive with anti-β-tubulin IV (Fig. 2b). In the apical zone, SCO ependymocytes projected protrusions into the SA containing mature secretory granules (Fig. 2d), which were strongly reactive with AFRU (Fig. 2e) and the lectin LFA (Fig. 2h). All SCO ependymocytes strongly reacted with anti-caveolin 1.

Hydrocephalic HTx fetuses As early as E15, the SCO of affected fetuses displayed abnormalities. In the middle third of the SCO, the cells had not differentiated into SCO ependymocytes (Figs. 1b, d, 2a). In the middle third, bundles of axons forming the posterior commissure were smaller and more numerous and lay closer to the ependymal layer as compared with the same region in the nHTx fetuses (compare Fig. 1c, d). At E18, the abnormality of the SCO-RF complex of hydrocephalic fetuses was evident (Fig. 1f, h). Immunostaining with AFRU and nestin revealed secretory ependymocytes in the rostral and caudal thirds of the SCO (Fig. 1h, j). The apical zone of SCO ependymocytes in these regions strongly bound the lectin LFA (Fig. 2k, inset). The cells lining the middle third of the SCO did not react with AFRU and nestin (Figs. 1h, j, 3e) but strongly expressed caveolin 1 (Fig. 3e). These cells neither displayed the subnuclear large cisternae of RER (Fig. 2j) nor secretory granules, as revealed by electron microscopy (Fig. 2l) and LFA binding (Fig. 2i). The abnormal phenotype of the SCO of hyHTx rats was confirmed by serial frontal sections taken through the whole length of the SCO and double-immunostained with AFRU and anti-β-tubulin IV (compare Fig. 3b–d/f–i, respectively).

SCO-RF complex of non-affected and hydrocephalic HTx rats after onset of hydrocephalus

By the end of the first postnatal week, non-affected rats displayed a RF running along the whole length of the central canal of the spinal cord, as revealed by double-immunolabelling with AFRU/anti-β-tubulin IV (Fig. 4c, e, g) and RAFRU/LFA binding (Fig. 4d). Along the central canal, RF establish contact with cilia of the ependymal cells (Fig. 4f, g). Hydrocephalic rats were devoid of RF as shown by double-immunolabelling with AFRU and anti-β-tubulin IV (Fig. 4h), Nomarski optics (Fig. 4i) and double-labelling with RAFRU and the lectin LFA (Fig. 4j). At PN7, the aqueduct was completely stenosed and the SCO was reduced to a small patch of secretory cells oriented upwards in the dilated third ventricle (Fig. 5a). Aggregated RF material could be seen in the third ventricle close to the SCO (Fig 5a, arrows, blue asterisk in large inset).

Stenosis of SA at the middle non-secretory third of SCO

All hydrocephalic rats from E19 to PN30 presented the middle non-secretory third of the SCO lying close to the ventral wall of the SA, resulting in marked stenosis (Figs. 4a, b, 5a). Transmission electron microscopy of the stenosed region of SA revealed a slender lumen, about 1 μm in width, to which ependymal cells projected microvilli and cilia (data not shown).

Changes in the protein composition of CSF

SCO-proteins At PN7, the CM-CSF of non-affected rats displayed AFRU+ bands of 200, 180, 164, 145, 120 and 63 kDa (Fig. 5c, d). In the LV-CSF from hydrocephalic PN7 rats, the 145- and 120-kDa bands were missing and two additional AFRU+ bands of 450 kDa and 320 kDa were

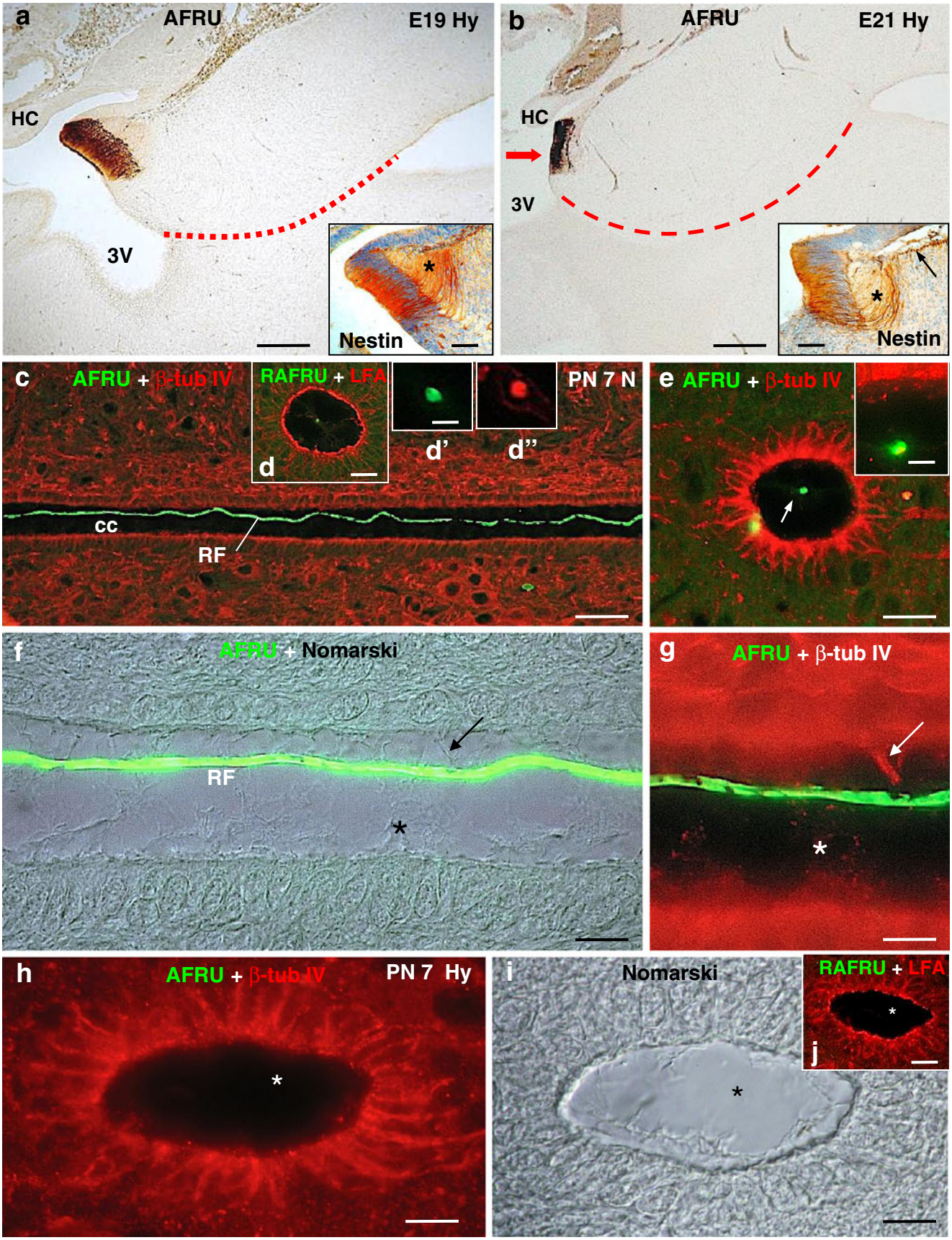
a
AFRU
E19 Hy
HC
3V
Nestin
b
AFRU
E21 Hy
HC
3V
Nestin
c
AFRU + β-tub IV
RAFRU + LFA
PN 7 N
d
d'
d''
cc
RF
e
AFRU + β-tub IV
f
AFRU + Nomarski
RF
g
AFRU + β-tub IV
h
AFRU + β-tub IV
PN 7 Hy
i
Nomarski
RAFRU + LFA
j

◀ **Fig. 4** In the hydrocephalic HTx rat, from E19 on, the Sylvius aqueduct (SA) becomes progressively stenosed and only the rostral third of the SCO remains differentiated and secretory. Postnatal hyHTx rats are devoid of Reissner's fibre. **a**, **b** In hydrocephalic E19 embryos, the middle non-secretory third of the SCO is situated close to the ventral wall of the SA (*dotted red line* in **a**). Only the rostral secretory third of the SCO remains active (*3V* third ventricle, *HC* habenular commissure). These secretory cells continue to project their basal processes (*asterisk*) towards the leptomeningeal space, as revealed by nestin immunostaining (*inset* in **a**). Shortly before birth (E21), the stenosis of the SA is more extensive (*broken red line* in **b**) and the small secretory SCO is oriented vertically overlooking the third ventricle (*red arrow* in **b**). These cells project their basal processes (*asterisk*) to the leptomeninges (*arrow*, *inset* in **b**). **c–g** By the end of the first postnatal week, non-hydrocephalic HTx rats are endowed with a Reissner's fibre (*RF*) running along the central canal (*cc*) of the spinal cord as shown by double-immunolabeling with AFRU (*green*) and β-IV-tubulin (*red*, in **c**, **e**, *inset* in **e**). Double-labelling with RAFRU (*green*) and the lectin LFA (affinity sialic acid residues; *red*) shows that the wall of the central canal is endowed with a thick layer of LFA-binding material (**d**) and that RF reacts with both AFRU (**d'**) and LFA (**d"**). Along the central canal, the RF establishes contact with the cilia of the ependymal cells (**f**, **g**). In **f**, the section is visualized with AFRU (*green*) and Nomarski optics by using the multichannel system Axio Vis Rel (Zeiss). In **g**, the same section is visualized with AFRU (*green*) and β-IV-tubulin (*red*). The same bundles of cilia shown in **f** (*arrow*, *asterisk*) are shown in **g**. **h**, **i** hyHTx rats are devoid of RF (*asterisk*) as shown by double-immunolabelling with AFRU (*green*) and β-IV-tubulin (*red*; **h**), Nomarski optics (**i**) and double-labelling with AFRU (*green*) and the lectin LFA (*red*; **j**). *Bars* 140 μm (**a**), 70 μm (*inset* in **a**), 180 μm (**b**), 70 μm (*inset* in **b**), 50 μm (**c**), 25 μm (**d**), 3.5 μm (**d'**, **d"**), 15 μm (**e**), 2.5 μm (*inset* in **e**), 10 μm (**f**, **g**), 10 μm (**h**, **i**), 15 μm (**j**)

detected (Fig. 5c, d, blue asterisks). The last-mentioned bands probably corresponded to RF material ectopically present in the ventricle (Fig. 5a, inset, arrows and blue asterisk). The density of the band of 200 kDa was significantly increased in the CM-CSF of hydrocephalic animals as compared with that of CM-CSF of non-affected rats and was significantly decreased in LV-CSF as compared with that of CM-CSF of non-affected and hydrocephalic rats (Fig. 5e). The CM-CSF collected from non-affected PN30 rats displayed AFRU reactive bands of 200, 63, 50 and 25 kDa (Fig. 5b). This pattern changed completely in the CM-CSF of hydrocephalic rats, since only the 63-kDa band was present (Fig. 5b). A marked difference in the pattern of AFRU immunoreactivity was also seen when hydrocephalic LV-CSF was compared with the non-affected and hydrocephalic CM-CSF. In the hydrocephalic LV-CSF, the bands of 200 and 63 kDa were more prominent and additional bands of 164, 120 and 50 kDa appeared (Fig. 5b).

The CM-CSF from non-affected rats collected at PN7 has additional AFRU+ compounds when compared with that collected at PN30 (compare Fig. 5b, c). The AFRU+ band pattern of CM-CSF of PN7 rats is similar to that of fetal CSF (see Vío et al. 2008). The AFRU+ 120-kDa compound can be regarded as a marker of the fetal SCO. This compound is missing in the CSF of hydrocephalic PN7 rats (Fig. 5c, d). On the other hand, the LV-CSF of PN30 hydrocephalic rats has additional AFRU+ bands as compared with that of PN7 hydrocephalic rats (compare Fig. 5b, d).

CSF proteome analysis The proteome profile was studied by using gel-based proteomics technology, in non-affected and hydrocephalic CSF collected at PN1 and PN7. The non-affected CSF was collected from the cisterna magna and the hydrocephalic CSF was collected from the lateral ventricles and cisterna magna. Non-affected and hydrocephalic CSF samples were aligned to obtain pairs for 2D gel analysis (Fig. 5f, g). Most protein spots were expressed in both normal and hydrocephalic samples but at different levels of expression, as shown by gel analysis (Figs. 5f, g, 6a) and densitometric analysis of spots (Fig. 6b, c). Most spots were present in both types of CSF samples at apparently the same concentration (Fig. 5f, g). However, spots 32, 33 and 37 were significantly increased in hydrocephalic CSF, whereas spots 1 and 12 were only detected in non-affected CSF (Fig. 5f) and spots 38, 39 and 40 were only detected in hydrocephalic CSF (Fig. 5g). The three spots (group 37) of 14 kDa but with a different isoelectric point reacted with anti-TTR, indicating that they corresponded to isoforms of TTR (Fig. 6e). This was confirmed by nanoLC-ESI-MS/MS (Fig. 6f). The latter method also revealed that spots 32 and 33 of about 40 kDa corresponded to TTR, most likely representing polymeric forms of the 14-kDa form (Fig. 6b). The three isoforms of the 14-kDa TTR form (spot 37) and the polymeric forms (spots 32 and 33) were significantly increased in the hydrocephalic LV-CSF as compared with the non-affected CM-CSF (Fig. 6a–c). The 14-kDa form of TTR was also increased in the CM-CSF of PN7 hydrocephalic rats as compared with the CM-CSF of PN7 non-affected rats (Fig. 6d).

Discussion

The stenosis of the SA is a key event for the development of fetal-onset hydrocephalus (Jones et al. 1987; Jones and Bucknall 1988; Bruni et al. 1988a, 1988b). The mechanism(s) responsible for this stenosis remains obscure. Overholser et al. (1954) have postulated that the secretion of the SCO prevents the closure of the SA and that maldevelopment of the SCO leads to SA stenosis and hydrocephalus. This hypothesis has been supported by findings obtained in animal models and human cases (Takeuchi and Takeuchi 1986; Takeuchi et al. 1987; Pérez-Fígares et al. 1998, 2001). The most direct evidence comes from the induction of SA stenosis and hydrocephalus by the immunoneutralization of the secretory proteins of the SCO during the fetal and postnatal periods of Sprague Dawley rats (Vío et al. 2000). The HTx rat is a genetic model of fetal-onset hydrocephalus in which stenosis of the SA and dilation of the lateral ventricles starts at E18 (Jones and Bucknall 1988;

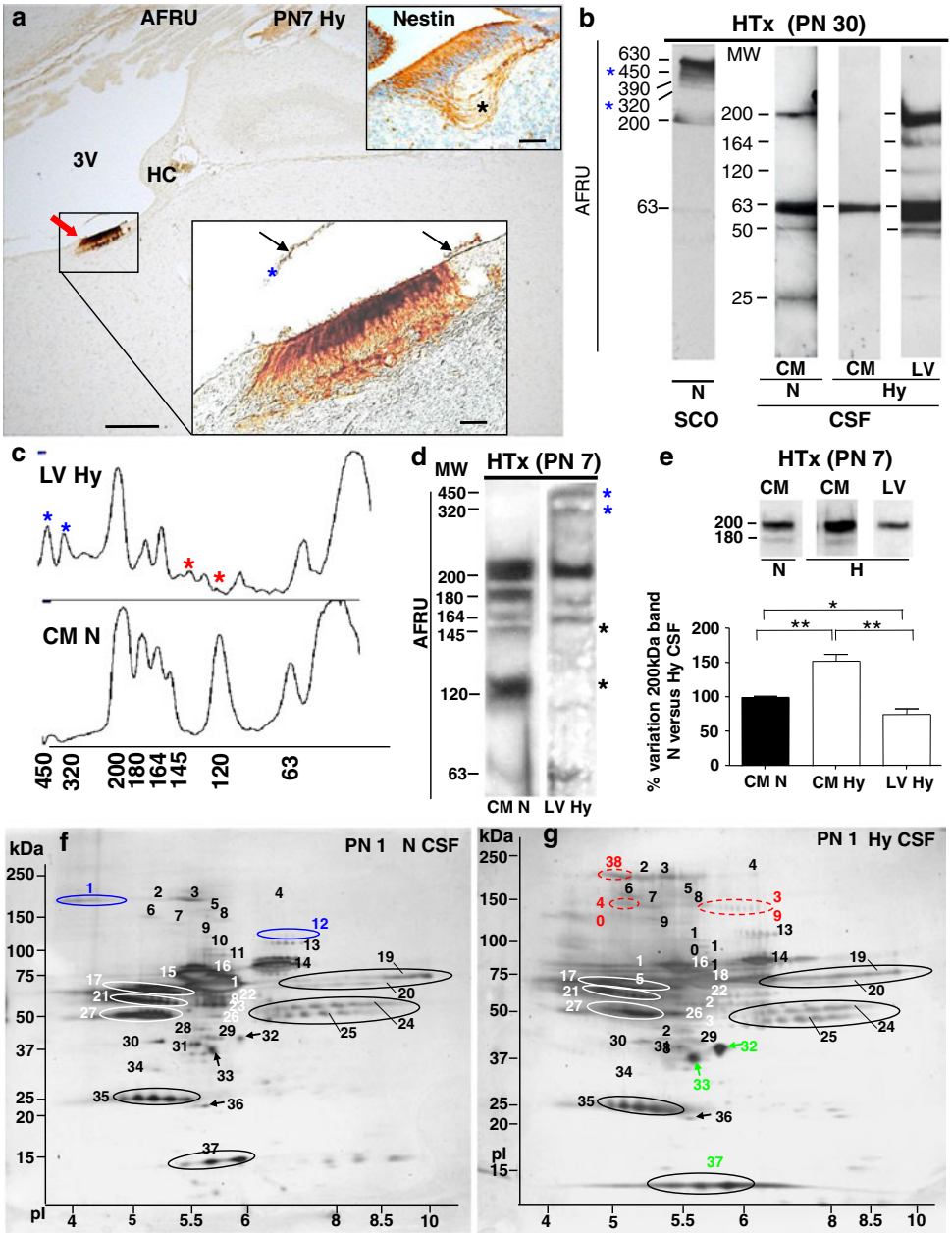

Fig. 5 Changes occur in the cerebrospinal fluid (CSF) proteins of hydrocephalic HTx rats. **a** Hydrocephalic rat at PN7 immunostained with AFRU. The SCO is reduced to a small patch of secretory cells (*red arrow*). The cells of the SCO have basal processes ending at the leptomeninges (*small inset*, *asterisk*). Note the aggregated RF material (*arrows* in *large inset*, *blue asterisk*). *Bars* 200 μm (**a**), 20 μm (*inset*). **b** Immunoblotting analysis of the SCO and CSF from non-affected (*N*) and hydrocephalic (*Hy*) rats collected at PN30 by using AFRU as the primary antibody (*numbers* molecular weight in kDa, *blue asterisks* secretory compounds also found in CSF from hydrocephalic HTx rats [see **c**]). CSF was collected from the cisterna magna (*CM*) in non-affected and hydrocephalic animals and from the lateral ventricles (*LV*) in hydrocephalic animals. **c** Densitometric linear scanning of the CSF immunoblots shown in **d**. **d** Immunoblotting analysis with AFRU of non-affected CM-CSF (*CM N*) and hydrocephalic LV-CSF (*LV Hy*) collected at PN7. In the hydrocephalic LV-CSF (**d**), note two compounds of 450 and 320 kDa (*blue asterisks*) not present in the non-affected CSF but corresponding to RF proteins (see *blue asterisks* in *inset* of **a** and in **b**, **c**) and two compounds that are missing (*black asterisks*) compared with non-affected CSF (see *red asterisks* in **c**). **e** The band of 200 kDa is significantly (***P*<0.001) increased in the CM-CSF of hydrocephalic animals as compared with their LV-CSF and with the CM-CSF of non-affected rats; this band was significantly decreased (**P*<0.05) in LV-CSF of hydrocephalic rats as compared with the CM-CSF of non-affected rats. Values are given as means ± SEM. **f**, **g** CSF proteome analysis. CSF from non-affected (*N*) and hydrocephalic (*Hy*) rats was analysed by two-dimensional chromatography and silver-staining. Note the spots present in the N CSF but missing in the Hy CSF (*highlighted in blue*), spots present in Hy CSF but missing in the N CSF (*highlighted in red*) and spots more optically dense in Hy CSF than in N CSF (*highlighted in green*)

Somera and Jones 2004). Here, we provide new evidence that the abnormal development of the SCO precedes the stenosis of the SA and that an alteration in the secretion of SCO glycoproteins can cause SA stenosis and hydrocephalus.

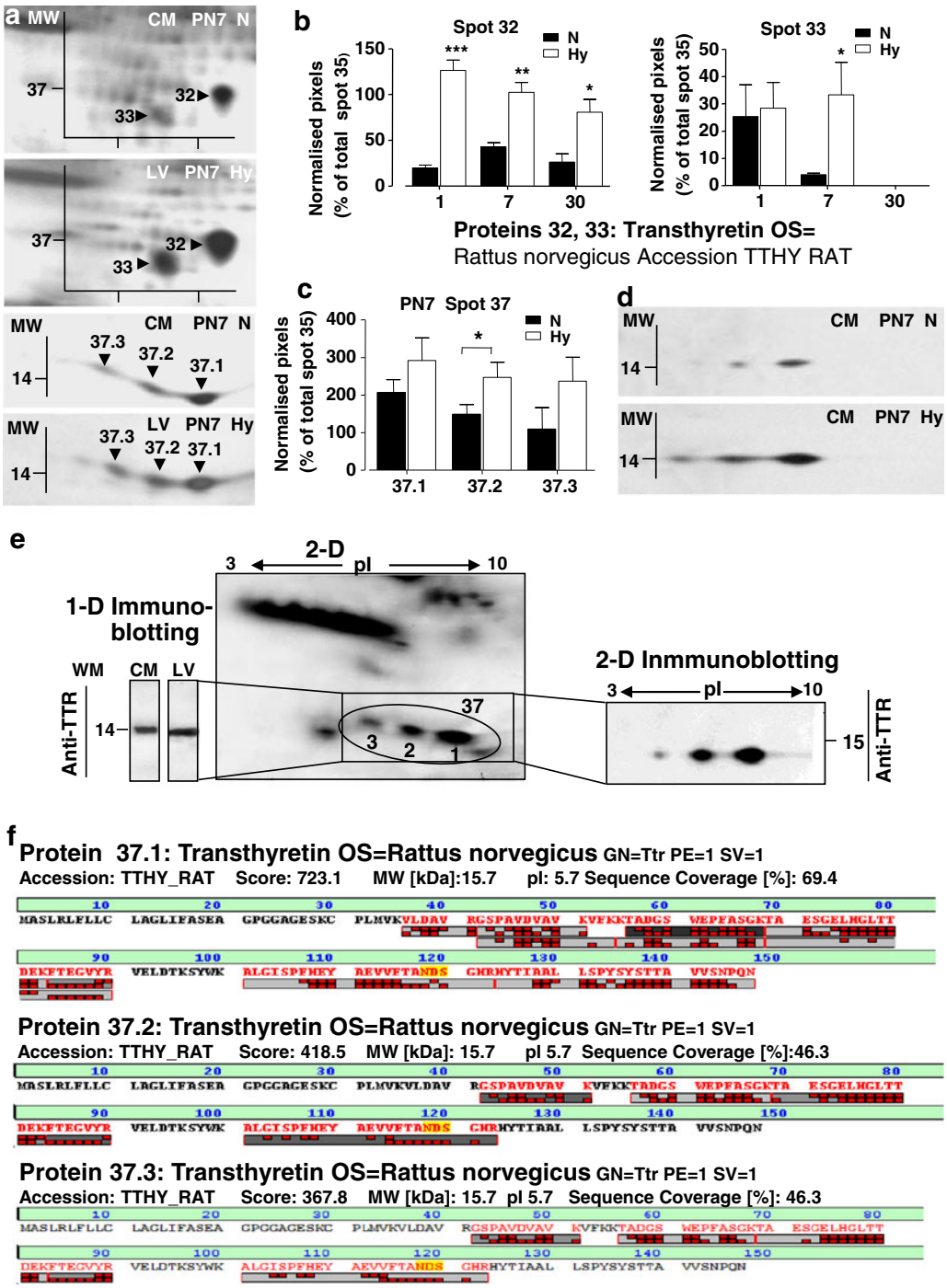

Fig. 6 Transthyretin (TTR) concentration is raised in the CSF of hydrocephalic HTx rats. CSF proteome analysis. **a** Comparative densitometric analysis of spots 32 and 33 and of spots 37.1, 37.2 and 37.3 from CM-CSF of non-affected PN7 rats and LV-CSF of PN7 hydrocephalic rats. The density of spots 32, 33 and 37 (1–3) was significantly increased in the hydrocephalic (*Hy*) CSF. **b** Quantitative densitometric analysis of spots 32 and 33. Since the density of the group of spots labelled "spot 35" was consistently similar in CSF samples from non-affected and hydrocephalic animals (see Fig. 5f, g), this density was regarded as 100% in order to evaluate increases or decreases of other spots that showed variability. In Hy CSF, the density of spot 32 is increased at PN1, PN7 and PN30. The density of spot 33 is increased at PN7 (PN30 samples were not studied). **P*<0.05; ***P*<0.01; ****P*<0.001. Values are given as means ± SEM. LC-ESI-MS/MS revealed that both spots corresponded to TTR. **c** Densitometry of the three isoforms of TTR (spots 37.1, 37.2, 37.3) in the CSF of non-affected (*N*) and hydrocephalic (*Hy*) rats at PN7. **P*<0.05. **d** Comparative two-dimensional (2D) electrophoresis of CM-CSF collected from non-affected (*N*) and hydrocephalic (*Hy*) rats at PN7. The three isoforms of TTR are increased in Hy CSF. **e** One (*1D*)- and two (*2D*)-dimensional electrophoresis and immunoblotting with anti-TTR of Hy CSF. Anti-TTR reacts with a band of 14 kDa in 1D blots. This band corresponds to the three spots (*1*, *2*, *3*) that have different isoelectric points (*pI*) and that react with anti-TTR. **f** LC_ESI-MS/MS analysis of spots 37 (1–3) reveals that the three proteins of 14 kDa correspond to isoforms of TTR

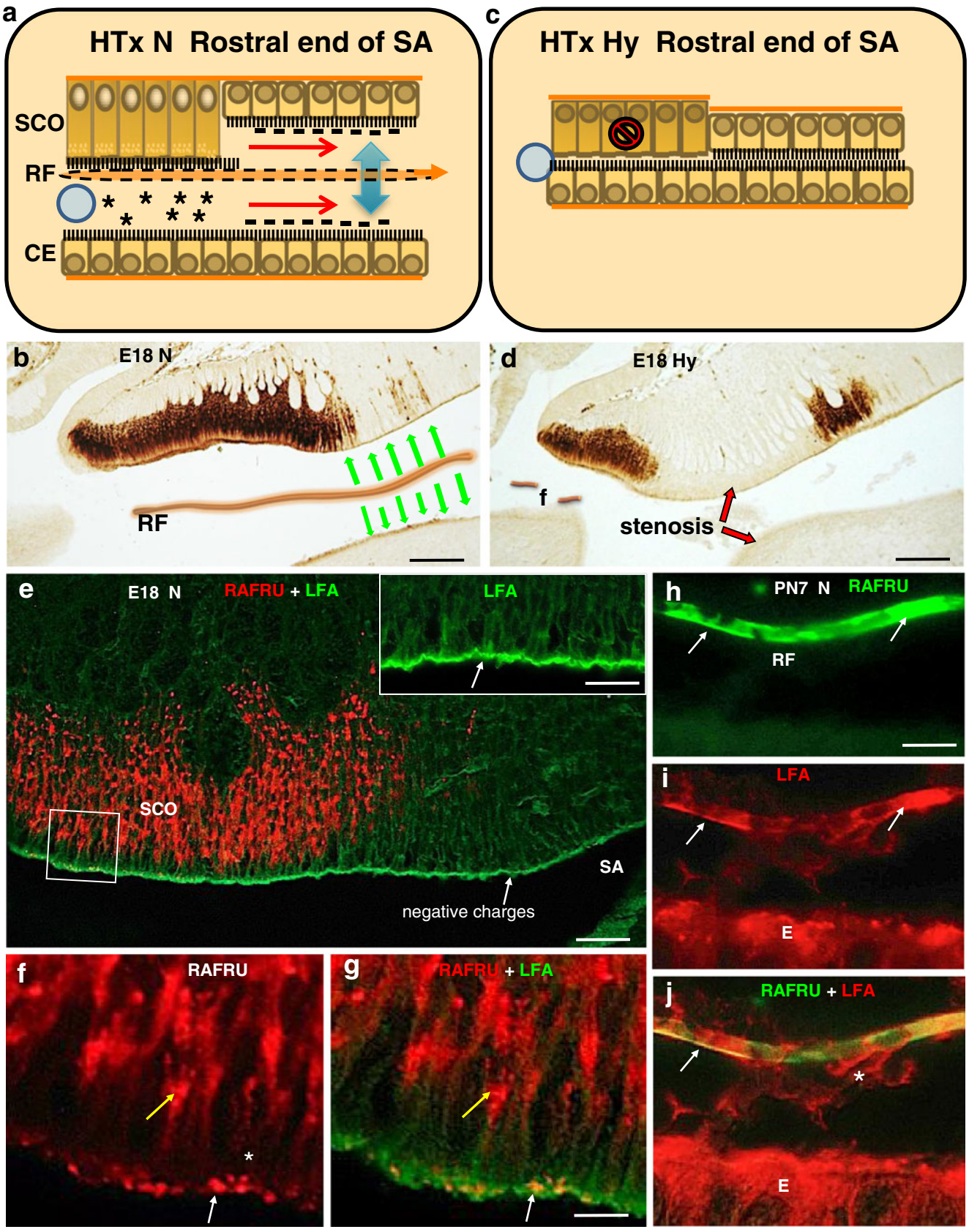
a
HTx N Rostral end of SA
SCO
RF
CE
c
HTx Hy Rostral end of SA
b
E18 N
RF
d
E18 Hy
f
stenosis
e
E18 N
RAFRU + LFA
LFA
SCO
SA
negative charges
h
PN7 N
RAFRU
RF
i
LFA
E
f
RAFRU
g
RAFRU + LFA
j
RAFRU + LFA
E

◀ **Fig. 7** Summary of our findings in non-affected and hydrocephalic HTx rats. **a** In the non-affected rat, the rostral end of the Sylvius aqueduct (*SA*) is lined ventrolaterally by multiciliated ependyma (*CE*) and dorsally by the subcommissural organ (*SCO*). The sialylated glycoproteins secreted by the SCO into the aqueduct form Reissner's fibre (*RF*) and also remain soluble in the CSF (*stars*). These negatively charged molecules and the RF proper contribute to keeping open this slender region of the aqueduct (*thick double-headed blued arrow*) allowing the flow of CSF (*light blue circle*) through the aqueduct (*red arrows*). **b** In the non-affected rat, the whole SCO secretes sialylated glycoproteins into the aqueduct forming a negatively charged layer on the surface of (1) the SCO (LFA binding), (2) the ventral wall of the aqueduct and (3) Reissner's fibre (*RF*), keeping the aqueduct open (*green arrows*) and allowing the flow of CSF. **c** In the hydrocephalic HTx rat, the middle third of the SCO does not secrete negatively charged molecules, RF does not form, the aqueduct becomes stenosed and the CSF does not flow. **d** The abnormal middle third of the SCO, lacking sialoglycoproteins, is the site at which aqueduct stenosis starts. Aggregated RF material (*f*) is only seen (displaced) in the third ventricle. **e–g** E18 embryo. Double-labelling with RAFRU (*red*) and the lectin LFA (affinity for sialic acid residues; *green*) shows that the surface of the subcommissural organ (*SCO*) and aqueduct (*SA*) strongly binds LFA (sialic acid residues = negative charges). *Inset* Detail of SA wall revealed only with the channel for *green* fluorescence. Note the thick coat of sialic acid residues (*arrow*). **f** Detail of *boxed area* in **e** with only the channel for *red* fluorescence (RAFRU) revealing the secretory proteins stored in RER cisternae (*yellow arrow*) and in apical secretory granules (*white arrow*). Note the subapical region (*asterisk*). **g** Same area as in **f** but merging both channels. Secretory proteins stored in RER do not bind LFA (*red*, *yellow arrow*) but those stored in the post-Golgi secretory granules do bind LFA (*white arrow*). **h–j** PN7 rat. Double-labelling with RAFRU (*green*) and the lectin LFA (affinity for sialic acid residues; *red*) shows that the periphery of Reissner's fibre (*RF*) reacts more strongly with RAFRU and binds more LFA (*arrows*) than the core of the fibre. **j** Merged image. *Yellow* surface of RF (*arrow*) corresponds to sialylated glycoproteins (*asterisk* apical processes of ependymal cells contacting RF, *E* ependymal cells). *Bars* 100 μm (**b**, **d**), 30 μm (**e**), 15 μm (inset in **e**), 7 μm (**f**, **g**), 5 μm (**h–j**)

Development of SCO is regulated by at least three different set of genes

The present findings in the hydrocephalic HTx rat suggest that the gene(s) mutated in the HTx is (are) involved in the development of only a discrete region of the SCO. Furthermore, in mutant mice such as the Msx1 strain (Fernández-Llebrez et al. 2004; Ramos et al. 2004), the transgenic mice RFX4_v3 and the fyn knockout mice (Blackshear et al. 2003; Baas et al. 2006; Rodríguez et al. 2007), only the rostral third of the SCO fully differentiates, whereas the middle and caudal regions fail to develop into a secretory structure. The neuroepithelium of the pretectal region, a prosomere 1 derivative, differentiates into the SCO. By analysing the expression of Pax3, Pax6 and Six3 in chicken and mouse (Ferran et al. 2008) and of cadherins (Redies et al. 2000), three pretectal domains in the anteroposterior axis have been distinguished and designated as precommissural, juxtacommissural and commissural. These three domains probably correspond to the three regions (rostral, middle and caudal) described in the SCO of the HTx rat (see above). A series of gain- or loss-of-function experiments performed in transgenic mice have helped to unfold the role played by various homeogenes and regulatory factors in the development of the SCO, including Pax6, Msx1, engrailed 1, Otx2, Dab2, RFX4 and SOCS (Louvi and Wassef 2000; Estivill-Torrus et al. 2001; Blackshear et al. 2003; Fernández-Llebrez et al. 2004; Krebs et al. 2004; Ramos et al. 2004; Zhang et al. 2007; Cheung et al. 2008; Huh et al. 2009; Larsen et al. 2010). The altered expression of these genes in the pretectal region leads to the abnormal development of the SCO and fetal-onset hydrocephalus. Taken as a whole, the evidence supports the conclusion that the development of the rostral, middle and caudal regions of the SCO is driven by three different sets of genes. This implies that the normal SCO should be composed of three different regions, supporting early studies that described a supracommissural, a precommissural and a subcommissural portion in the rodent and primate SCO (Palkovitts 1965; Hofer 1976). Although the genes that are responsible for hydrocephalus in the HTx rat have not yet been identified, a quantitative trait analysis has shown that the loci associated with the hydrocephalus phenotype exist on chromosomes 9, 10, 11 and 17 (Jones et al. 2004). Gene arrays studies have found a relatively low number of transcripts to be altered in this model, such as kolecystokinin, nuclear factor 1, galectin-3, xanthine dehydrogenase and tumor necrosis factor (Miller et al. 2006). No information is available on whether these altered proteins are involved in the abnormal development of the SCO of the hydrocephalic HTx rat. Thus, the genetic basis of such a distinct malformation of the SCO of this rat strain remains unsolved.

Hydrocephalic HTx rats lack RF

The polymerization of RF-glycoproteins is a complex process that is poorly understood. Briefly, the released proteins first aggregate into fibrils arranged as a film that covers the surface of the SCO (pre-RF) and the floor of the SA and then undergo a higher degree of aggregation to form RF (Rodríguez et al. 1987). Since the hydrocephalic HTx rats lack RF, such a mechanism presumably does not operate in this mutant. Why are these rats unable to form a RF despite (1) their retention of a rostral portion of the SCO that is actively secreting and (2) their narrowed but open SA? The middle and caudal regions of the SCO, which are absent in these rats during pre- and postnatal life, are probably necessary for RF assembly. Do these two regions of SCO secrete compounds different from those secreted by the rostral region of the SCO? The changes found in the AFRU+ proteins in the hydrocephalic CSF suggest a positive answer (see below).

Abnormal development of the SCO triggers SA stenosis and hydrocephalus

In the non-affected rat, differentiation of the SCO starts at E12-E13 (Schoebitz et al. 1993); this process is altered in the hydrocephalic HTx rat. In these rats, a distinct malformation of the SCO is present as early as E15 (present investigation). Since stenosis of the SA occurs at E18 and dilation of the lateral ventricles starts at E19, malformation of the SCO clearly precedes the onset of hydrocephalus, supporting the findings by Somera and Jones (2004).

SCO ependymocytes are highly differentiated cells with a distinct zonation of the cytoplasm. The supranuclear region contains flattened cisternae of RER and the Golgi apparatus, the large subnuclear RER cisternae store the precursor forms of the secretory proteins, the subapical zone contains bundles of microtubules transporting the secretory granules and the apical region contains mature secretory granules (Rodríguez et al. 1992, 1998). The absence of this organization of the secretory pathway in the cells forming the middle third of the SCO of the hydrocephalic HTx rat and the lack of AFRU immunoreactivity of these cells indicate that this region of the abnormal SCO is not secreting RF proteins.

The absence of RF in the hydrocephalic HTx rat will have at least two consequences. First, we hypothesize that the sialylated glycoproteins secreted by the SCO provide a large mass of negatively charged molecules that help to keep the SA open (Fig. 7; see also Wagner et al. 2003). During prenatal life, negative charges are provided by the CSF-soluble sialylated glycoproteins secreted by the SCO (Fig. 7e), whereas during postnatal life, these charges are provided by the sialoglycoproteins forming RF (Fig. 7h–j). In the hyHTx rat, the lack of secretions from the middle and caudal regions of the SCO largely diminishes the negative charges in the SA domain and this contributes to SA stenosis (Fig. 7). The absence of RF and consequently of the negative charges of sialic acid, is a common feature among the various animal models in which the abnormal development of the SCO-RF complex leads to aqueductal stenosis and fetal onset hydrocephalus (Rodríguez et al. 2007). Furthermore, the absence of RF implies the loss of the bulk of SCO-spondin, the major constitutive protein of RF that displays 26 thrombospondin type I repeats with antiadhesive properties (Gobron et al. 1996; Monnerie et al. 1998; Meiniel 2001). Etus and Belce (2003) have reported a decrease of sialic acid content in periventricular areas of mature rats with hydrocephalus induced by the injection of kaolin into the cisterna magna. This change in sialic acid resulting from an induced hydrocephalus is certainly not related to the physiopathology underlying the onset of congenital hydrocephalus.

A second consequence of the absence of RF in the hydrocephalic HTx rat would be on the CSF hydrodynamics. The fresh untreated bovine RF has a 97.3% water content and is 50 μm in diameter (Rodríguez et al. 1984a). Thus, in the living animal, RF occupies a large proportion of the SA lumen. A single injection of anti-RF antibodies into the CSF interrupts the formation of RF (Rodríguez et al. 1990) and leads to a reduction of the bulk flow of CSF through the central canal of the spinal cord (Cifuentes et al. 1994). The absence of RF in the SA of the hydrocephalic HTx rat might thus also interfere with the bulk flow of CSF through the aqueduct (Fig. 7). This possibility is supported by the following findings: (1) horseradish peroxidase, a 42-kDa marker protein, when injected into a lateral ventricle of a PN5 hydrocephalic HTx rat does not move through the stenosed SA (own unpublished observation); (2) immunoneutralization of the SCO-RF complex during the fetal and postnatal periods in normal rats results in SA stenosis and hydrocephalus (Vío et al. 2000). Thus, RF appears as a key element for normal CSF flow through the SA. This may help us to understand why the SCO-RF complex, an ancient structure in evolution, is situated at the "right" place, namely the entrance of the SA.

Changes in the proteome of CSF of hyHTx rats

The comparative analysis of the proteome of CSF collected from non-affected rats and hydrocephalic littermates has revealed that many proteins are present in both types of CSF, whereas others are missing either in the normal CSF or in the hydrocephalic CSF and yet others are present in both types of CSF but at a higher concentration in the hydrocephalic CSF. These differences can neither be explained by abnormal clearance nor by a dilution factor of the large CSF volume, since many proteins are present in both types of CSFs at similar concentrations, whereas others are increased or decreased in the hydrocephalic CSF. Instead, abnormalities in the secretion of proteins that are normally released into the CSF, such as those of the SCO (SCO-spondin) and choroid plexus (TTR), might contribute to the abnormal protein composition of the hydrocephalic CSF. The present investigation has focused on these proteins. Studies are in progress to identify the other proteins whose presence in the CSF of the hydrocephalic HTx rat is altered.

Abnormalities in SCO secretion The 200-kDa AFRU+ protein present in the CSF of nHTx rats has been regarded as a processed form of SCO-spondin (Vío et al. 2008). The presence of this protein in the hydrocephalic CSF and the absence of RF indicate that the small portion of SCO remaining in the hydrocephalic HTx rat secretes SCO-spondin as a processed CSF-soluble protein. The

significance of this protein in the non-hydrocephalic CSF and hydrocephalic CSF remains to be investigated. Worth considering is the finding that SCO-spondin promotes neuronal growth and differentiation (Monnerie et al. 1998; Meiniel 2001). The hydrocephalic CSF of the lateral ventricles of PN7 rats contains AFRU+ proteins of 450 and 320 kDa. In the nHTx rat, these proteins are present in the SCO proper but not in the RF or CSF (Vío et al. 2008) and correspond to partially processed forms. This indicates that the SCO of hyHTx rats releases immature forms of RF-proteins into the CSF. At PN30, out of the four bands consistently revealed by AFRU in the CSF of the cisterna magna in nHTx rats, only one (63 kDa) is present in the CSF collected from the cisterna magna of hyHTx rats. How did the 63-kDa protein reach the cisterna magna? We hypothesize that the basal processes of the SCO ependymocytes of HTx rats projecting towards the subarachnoid space (basal route of secretion; Rodríguez et al. 1984b) could be the pathway by which the 63-kDa protein reaches the cisternal CSF. Furthermore, at PN30, the CSF of the lateral ventricle of hyHTx rats contains more forms of AFRU+ compounds and at a higher concentration than the CSF from cisterna magna of nHTx, suggesting that these proteins are secreted by the rostral end of the SCO and that they are not efficiently cleared from the CSF of hyHTx rats. The findings indicate that not only the absence of RF but also the lack of flow through the SA of sialylated SCO secretory proteins and the presence in the CSF of abnormal forms of SCO secretory proteins contribute to SA stenosis.

TTR concentration in the CSF of non-affected and hydrocephalic HTx rats In the CSF of hyHTx rats, the TTR concentration is higher than in the CSF of nHTx rats. This should be ascribed to a higher rate of secretion and not to a reduced clearance, since the CSF concentration of other proteins either decreases or does not change at all. What is the source of the TTR present in the CFS of the hyHTx rats? Under normal conditions, the main source of CSF-TTR is the choroid plexus (Johanson et al. 2008). The choroid plexus of the hyHTx rat probably secretes TTR into the CSF at a higher rate in comparison with the nHTx rat. In this context, factors that modulate TTR levels in the hydrocephalic CSF could be important to consider in hydrocephalus. The findings that RF-glycoproteins have specific binding sites in the choroid plexus (Miranda et al. 2001) and that the CSF concentration of these proteins is increased in the hydrocephalic CSF, have to be kept in mind. The SCO is also a source of CSF-TTR (Rodríguez et al. 2001; Montecinos et al. 2005). However, the small group of SCO secretory cells present in the hyHTx rat are probably not responsible for the increased levels of TTR in the CSF. Additionally, information has been obtained that, under normal conditions, neurons can contribute to the CSF levels of TTR (Li et al. 2011) and that such a contribution increases substantially under certain pathological states, such as Aβ pathology (Buxbaum et al. 2008; Li and Buxbaum 2011). The possibility of a neuronal origin of the increased levels of TTR in the CSF of the hyHTx rat, which also displays brain pathology (Mashayekhi et al. 2002), must also be considered.

TTR-committed functions in the CNS have not been completely addressed. A growing number of reports shows additional TTR roles other than the transport of T4 (Woeber and Ingbar 1986) and retinol (Kanai et al. 1968), such as its involvement in normal brain development (Schreiber 2002; Richardson et al. 2007; Fleming et al. 2009). Furthemore, evidence has been provided that TTR has beneficial effects on neurodegenerative processes such Aβ and Tau-associated pathology (Li and Buxbaum 2011). We speculate that the increased production of TTR in the hyHTx rat is involved in neuroprotection.

Concluding remarks

In the hydrocephalic HTx rats, a distinct malformation of the SCO is present as early as E15. Since stenosis of the SA occurs at E18 and dilation of the lateral ventricles starts at E19, the malformation of the SCO clearly precedes the onset of hydrocephalus. The abnormal development of the SCO results in changes in the protein composition of CSF and the absence of RF. Since the SCO is the source of a large mass of sialylated glycoproteins that form RF and those that remain CSF-soluble, we hypothesize that the absence of this large mass of negatively charged molecules from the SA domain results in SA stenosis, impairs the bulk flow of CSF through the aqueduct and causes severe hydrocephalus. The proteomic screening of CSF has revealed differences in the CSF proteins of non-affected and hydrocephalic rats, in particular with respect to SCO-secretory proteins and TTR.

Acknowledgments The authors acknowledge the valuable technical support of Mr. Genaro Alvial. The monoclonal antibody against nestin was obtained from the Developmental Studies Hybridoma Bank developed under the auspices of the NICHD and maintained by The University of Iowa, Department of Biological Sciences, Iowa City, IA 52242.

References

Baas D, Meiniel A, Benadiba C, Bonnafe E, Meiniel O, Reith W, Durand B (2006) A deficiency in RFX3 causes hydrocephalus associated with abnormal differentiation of ependymal cells. Eur J Neurosci 24:1020–1030

Blackshear PJ, Graves JP, Stumpo DJ, Cobos I, Rubenstein JL, Zeldin DC (2003) Graded phenotypic response to partial and complete deficiency of a brain-specific transcript variant of

the winged helix transcription factor RFX4. Development 130:4539–4552

Bruni JE, Del Bigio MR, Cardoso ER, Persaud TV (1988a) Hereditary hydrocephalus in laboratory animals and humans. Exp Pathol 35:239–246

Bruni JE, Del Bigio MR, Cardoso ER, Persaud TV (1988b) Neuropathology of congenital hydrocephalus in the SUMS/NP mouse. Acta Neurochir (Wien) 92:118–122

Buxbaum JN, Ye Z, Reixach N, Friske L, Levy C, Das P, Golde T, Masliah E, Roberts AR, Bartfai T (2008) Transthyretin protects Alzheimer's mice from the behavioral and biochemical effects of Aβ toxicity. Proc Natl Acad Sci USA 105:2681–2686

Caprile T, Hein S, Rodríguez S, Montecinos H, Rodríguez EM (2003) Reissner fiber binds and transports away monoamines present in the cerebrospinal fluid. Brain Res Mol Brain Res 110:177–192

Chae TH, Kim S, Marz KE, Hanson PI, Walsh CA (2004) The hyh mutation uncovers roles for alpha Snap in apical protein localization and control of neural cell fate. Nat Genet 36:264–270

Cheung KK, Mok SC, Rezaei P, Chan WY (2008) Dynamic expression of Dab2 in the mouse embryonic central nervous system. BMC Dev Biol 8:76

Cifuentes M, Rodríguez S, Pérez J, Grondona JM, Rodríguez EM, Fernández-Llebrez P (1994) Decreased cerebrospinal fluid flow though the central canal of the spinal cord of rats immunologically deprived of Reissner's fibre. Exp Brain Res 98:431–440

Estivill-Torrus G, Vitalis T, Fernández-Llebrez P, Price DJ (2001) The transcription factor Pax6 is required for development of the diencephalic dorsal mid-line secretory radial glia that form the subcommissural organ. Mech Dev 109:215–224

Etus V, Belce A (2003) Total sialic acid levels decrease in the periventricular area of infantile rats with hydrocephalus. Childs Nerv Syst 19:825–828

Fernández-Llebrez P, Grondona JM, Pérez J, López-Aranda MF, Estivill-Torrus G, Llebrez-Zayas PF, Soriano E, Ramos C, Lallemand Y, Bach A, Robert B (2004) Msx1-deficient mice fail to form prosomere 1 derivatives, subcommissural organ, and posterior commissure and develop hydrocephalus. J Neuropathol Exp Neurol 63:574–586

Ferran JL, Sánchez-Arrones L, Bardet SM, Sandoval JE, Martínez-de-la-Torre M, Puelles L (2008) Early pretectal gene expression pattern shows a conserved anteroposterior tripartition in mouse and chicken. Brain Res Bull 75:295–298

Fleming CE, Mar FM, Franquinho F, Saraiva MJ, Sousa MM (2009) Transthyretin internalization by sensory neurons is megalin mediated and necessary for its neuritogenic activity. J Neurosci 29:3220–3232

Gobron S, Monnerie H, Meiniel R, Creveaux I, Lehmann W, Lamalle D, Dastugue B, Meiniel A (1996) SCO-spondin: a new member of the thrombospondin family secreted by the subcommissural organ is a candidate in the modulation of neuronal aggregation. J Cell Sci 109:1053–1061

Gobron S, Creveaux I, Meiniel R, Didier R, Herbet A, Bamdad M, El Bitar F, Dastugue B, Meiniel A (2000) Subcommissural organ/Reissner's fiber complex: characterization of SCO-spondin, a glycoprotein with potent activity on neurite outgrowth. Glia 32:177–191

Hofer H (1976) Beobachtungen an dem Sogenannten "Supracommissuralen Organ" (Fuse) und am Recessus Mesocoelicus der Primaten. Folia Primatol 5:190–200

Hoyo-Becerra C, Lopez-Avalos MD, Perez J, Miranda E, Rojas-Rios P, Fernández-Llebrez P, Grondona JM (2006) Continuous delivery of a monoclonal antibody against Reissner's fiber into CSF reveals CSF-soluble material immunorelated to the subcommissural organ in early chick embryos. Cell Tissue Res 326:771–786

Huh MS, Todd MA, Picketts DJ (2009) SCO-ping out the mechanisms underlying the etiology of hydrocephalus. Physiology (Bethesda) 24:117–126

Johanson CE, Duncan JA III, Klinge PM, Brinker T, Stopa EG, Silverberg GD (2008) Multiplicity of cerebrospinal fluid functions: new challenges in health and disease. Cerebrospinal Fluid Res 5:10

Jones HC, Bucknall RM (1988) Inherited prenatal hydrocephalus in the H-Tx rat: a morphological study. Neuropathol Appl Neurobiol 14:263–274

Jones HC, Dack S, Ellis C (1987) Morphological aspects of the development of hydrocephalus in a mouse mutant (SUMS/NP). Acta Neuropathol 72:268–276

Jones HC, Depelteau JS, Carter BJ, Somera KC (2002) The frequency of inherited hydrocephalus is influenced by intrauterine factors in H-Tx rats. Exp Neurol 176:213–220

Jones HC, Yehia B, Chen GF (2004) Genetic analysis of inherited hydrocephalus in a rat model. Exp Neurol 190:79–90

Kanai M, Raz A, Goodman DS (1968) Retinol-binding protein: the transport protein for vitamin A in human plasma. J Clin Invest 47:2025–2044

Krebs DL, Metcalf D, Merson TD, Voss AK, Thomas T, Zhang JG, Rakar S, O'Bryan MK, Willson TA, Viney EM, Mielke LA, Nicola NA, Hilton DJ, Alexander WS (2004) Development of hydrocephalus in mice lacking SOCS7. Proc Natl Acad Sci USA 101:15446–15451

Lang B, Song B, Davidson W, MacKenzie A, Smith N, McCaig CD, Harmar AJ, Shen S (2006) Expression of the human PAC1 receptor leads to dose-dependent hydrocephalus-related abnormalities in mice. J Clin Invest 116:1924–1934

Larsen KB, Lutterodt MC, Møllgård K, Møller M (2010) Expression of the homeobox genes OTX2 and OTX1 in the early developing human brain. J Histochem Cytochem 58:669–678

Li X, Buxbaum JN (2011) Transthyretin and the brain re-visited: is neuronal synthesis of transthyretin protective in Alzheimer's disease? Mol Neurodegener 6:79

Li X, Masliah E, Reixach N, Buxbaum JN (2011) Neuronal production of transthyretin in human and murine Alzheimer's disease: is it protective? J Neurosci 31:12483–12490

Louvi A, Wassef M (2000) Ectopic engrailed 1 expression in the dorsal midline causes cell death, abnormal differentiation of circumventricular organs and errors in axonal pathfinding. Development 127:4061–4071

Mashayekhi F, Draper CE, Bannister CM, Pourghasem M, Owen-Lynch PJ, Miyan JA (2002) Deficient cortical development in the hydrocephalic Texas (H-Tx) rat: a role for CSF. Brain 125:1859–1874

Meiniel A (2001) SCO-spondin, a glycoprotein of the subcommissural organ/Reissner's fiber complex: evidence of a potent activity on neuronal development in primary cell cultures. Microsc Res Tech 52:484–495

Miller JM, Kumar R, McAllister JP II, Krause GS (2006) Gene expression analysis of the development of congenital hydrocephalus in the H-Tx rat. Brain Res 1075:36–47

Miranda E, Almonacid JA, Rodriguez S, Perez J, Hein S, Cifuentes M, Fernández-Llebrez P, Rodríguez EM (2001) Searching for specific binding sites of the secretory glycoproteins of the subcommissural organ. Microsc Res Tech 52:541–551

Monnerie H, Dastugue B, Meiniel A (1998) Effect of synthetic peptides derived from SCO-spondin conserved domains on chick cortical and spinal-cord neurons in cell cultures. Cell Tissue Res 293:407–418

Montecinos HA, Richter H, Caprile T, Rodríguez EM (2005) Synthesis of transthyretin by the ependymal cells of the subcommissural organ. Cell Tissue Res 320:487–499

Overholser MD, Whitley JR, O'Dell BL, Hogan AG (1954) The ventricular system in hydrocephalic rat brains produced by a

deficiency of vitamin B12 or of folic acid in the maternal diet. Anat Rec 120:917–934

Palkovitts M (1965) Morphology and function of the subcommissural organ. Stud Biol Acad Sci Hung 4:1–103

Pérez-Fígares JM, Jiménez AJ, Pérez-Martín M, Fernández-Llebrez P, Cifuentes M, Riera P, Rodríguez S, Rodríguez EM (1998) Spontaneous congenital hydrocephalus in the mutant mouse hyh. Changes in the ventricular system and the subcommissural organ. J Neuropathol Exp Neurol 57:188–202

Pérez-Fígares JM, Jiménez AJ, Rodríguez EM (2001) Subcommissural organ, cerebrospinal fluid circulation, and hydrocephalus. Microsc Res Tech 52:591–607

Peruzzo B, Rodríguez S, Delannoy L, Hein S, Rodríguez EM (1987) Ultrastructural immunocytochemical study of the massa caudalis of lamprey larvae (*Geotria australis*). Evidence for the vascular fate of Reissner's fiber material. Cell Tissue Res 247:367–376

Picketts DJ (2006) Neuropeptide signaling and hydrocephalus: SCO with the flow. J Clin Invest 116:1828–1832

Ramos C, Fernández-Llebrez P, Bach A, Robert B, Soriano E (2004) Msx1 disruption leads to diencephalon defects and hydrocephalus. Dev Dyn 230:446–460

Redies C, Ast M, Nakagawa S, Takeichi M, Martinez-de-la-Torre M, Puelles L (2000) Morphologic fate of diencephalic prosomeres and their subdivisions revealed by mapping cadherin expression. J Comp Neurol 421:481–514

Richardson SJ, Lemkine GF, Alfama G, Hassani Z, Demeneix BA (2007) Cell division and apoptosis in the adult neural stem cell niche are differentially affected in transthyretin null mice. Neurosci Lett 421:234–238

Rodríguez S, Caprile T (2001) Functional aspects of the subcommissural organ-Reissner's fiber complex with emphasis in the clearance of brain monoamines. Microsc Res Tech 52:564–572

Rodríguez EM, Oksche A, Hein S, Rodríguez S, Yulis CR (1984a) Comparative immunocytochemical study of the subcommissural organ. Cell Tissue Res 237:427–441

Rodríguez EM, Oksche A, Hein S, Rodríguez S, Yulis CR (1984b) Spatial and structural interrelationships between secretory cells of the subcommissural organ and blood vessels. An immunocytochemical study. Cell Tissue Res 237:443–449

Rodríguez EM, Oksche A, Rodríguez S, Hein S, Peruzzo B, Schöbitz K, Herrera H (1987) The subcommissural organ-Reissner's fiber unit. In: Gross PM (ed) Circumventricular organs and body fluids, vol II. CRC Press, Florida, pp 1–41

Rodríguez S, Rodríguez EM, Jará P, Peruzzo B, Oksche A (1990) Single injection into the cerebrospinal fluid of antibodies against the secretory material of the subcommissural organ reversibly blocks formation of Reissner's fiber: immunocytochemical investigations in the rat. Exp Brain Res 81:113–124

Rodríguez EM, Oksche A, Hein S, Yulis CR (1992) Cell biology of the subcommissural organ. Int Rev Cytol 135:39–121

Rodríguez EM, Rodríguez S, Hein S (1998) The subcommissural organ. Microsc Res Tech 41:98–123

Rodríguez S, Vío K, Wagner C, Barría M, Navarrete EH, Ramírez VD, Pérez-Fígares JM, Rodríguez EM (1999) Changes in the cerebrospinal-fluid monoamines in rats with an immunoneutralization of the subcommissural organ-Reissner's fiber complex by maternal delivery of antibodies. Exp Brain Res 128:278–290

Rodríguez EM, Oksche A, Montecinos H (2001) Human subcommissural organ, with particular emphasis on its secretory activity during the fetal life. Microsc Res Tech 52:573–590

Rodríguez S, Bátiz F, Ortloff A, Vío K, Muñoz RI, DeGraff LM, Graves JP, Stumpo DJ, Blackshear PJ, Zeldin DC, Goto J, Tezuka T, Yamamoto Y, Rodríguez EM (2007) Lack of formation of Reissner fiber leads to hydrocephalus. Cerebrospinal Fluid Research 4 (Suppl 1):S25

Schoebitz K, Garrido O, Heinrichs M, Speer L, Rodríguez EM (1986) Ontogenetical development of the chick and duck subcommissural organ. An immunocytochemical study. Histochemistry 84:31–40

Schoebitz K, Rodríguez EM, Garrido O, Del Brio Leon MA (1993) Ontogenetic development of the subcommissural organ with reference to the flexural organ. In: Oksche A, Rodriguez EM, Fernandez-Llebrez P (eds) The subcommissural organ, an ependymal brain gland. Springer, Berlin, pp 41–49

Schreiber G (2002) The evolutionary and integrative roles of transthyretin in thyroid hormone homeostasis. J Endocrinol 175:61–73

Shevchenko A, Wilm M, Vorm O, Mann M (1996) Mass spectrometric sequencing of proteins from silver stained polyacrylamide gels. Anal Chem 68:850–858

Somera KC, Jones HC (2004) Reduced subcommissural organ glycoprotein immunoreactivity precedes aqueduct closure and ventricular dilatation in H-Tx rat hydrocephalus. Cell Tissue Res 315:361–373

Sternberger LA, Hardy PH, Cuculis JJ, Meyer HG (1970) The unlabeled antobody enzyme method of immunohistochemistry. Preparation and properties of soluble antigen-antibody complex (horseradish peroxidase-antihorseradish peroxidase) and its use in identification of spirochetes. J Histochem Cytochem 18:315–333

Takeuchi IK, Takeuchi YK (1986) Congenital hydrocephalus following X-irradiation of pregnant rats on an early gestational day. Neurobehav Toxicol Teratol 8:143–150

Takeuchi IK, Kimura R, Matsuda M, Shoji R (1987) Absence of subcommissural organ in the cerebral aqueduct of congenital hydrocephalus spontaneously occurring in MT/HokIdr mice. Acta Neuropathol 73:320–322

Towbin H, Staehelin T, Gordon J (1979) Electrophoretic transfer of proteins from polyacrylamide gels to nitrocellulose sheets: procedure and some applications. Proc Natl Acad Sci USA 76:4350–4354

Vío K, Rodríguez S, Navarrete EH, Pérez-Fígares JM, Jiménez AJ, Rodríguez EM (2000) Hydrocephalus induced by immunological blockage of the subcommissural organ-Reissner's fiber (RF) complex by maternal transfer of anti-RF antibodies. Exp Brain Res 135:41–52

Vío K, Rodríguez S, Yulis CR, Oliver C, Rodríguez EM (2008) The subcommissural organ of the rat secretes Reissner's fiber glycoproteins and CSF-soluble proteins reaching the internal and external CSF compartments. Cerebrospinal Fluid Res 5:1–14

Wagner C, Bátiz LF, Rodríguez S, Jiménez AJ, Páez P, Tomé M, Pérez-Fígares JM, Rodríguez EM (2003) Cellular mechanisms involved in the stenosis and obliteration of the cerebral aqueduct of hyh mutant mice developing congenital hydrocephalus. J Neuropathol Exp Neurol 62:1019–1040

Woeber KA, Ingbar SH (1986) The contribution of thyroxine-binding prealbumin to the binding of thyroxine in human serum, as assessed by immunoadsorption. J Clin Invest 47:1710–1721

Zhang D, Zeldin DC, Blackshear PJ (2007) Regulatory factor X4 variant 3: a transcription factor involved in brain development and disease. J Neurosci Res 85:3515–3522